Publications

3-23-2007

Doppler Ducting of Short-Period Gravity Waves by Midaltitude Tidal Wind Structure

Jonathan B. Snively
The Pennsylvania State University, snivelyj@erau.edu

Victor P. Pasko
The Pennsylvania State University

Michael J. Taylor
Utah State University

Wayne K. Hocking
University of Western Ontario

Doppler ducting of short-period gravity waves by midlatitude tidal wind structure

Jonathan B. Snively,[1] Victor P. Pasko,[1] Michael J. Taylor,[2] and Wayne K. Hocking[3]

[1] Multiwavelength airglow image data depicting a short-period ($\sim$4.9 min) atmospheric gravity wave characterized by a sharp leading front have been analyzed together with synoptic meteor radar wind data recorded simultaneously from Bear Lake Observatory, Utah (41.6°N, 111.6°W). The wind data suggest the presence of a semidiurnal tide with horizontal winds peaking at around 60 m/s along the SSE direction of motion (170° from north) of this short-period wave. It was found that the gravity wave was most probably ducted because of the Doppler shift imposed by this wind structure. A marked 180° phase shift was observed between the near-infrared OH and the OI (557.7 nm) emissions. Numerical simulation results for similar ducted waves excited by idealized model sources suggest that the phase shift between the wave-modulated airglow intensities may be explained simply by chemical processes rather than by wave dynamics. Phase velocities of simulated waves, however, appear higher than those of observed waves, suggesting the importance of tidal thermal structure in determining the Doppler-ducted wave characteristics.

1. Introduction

[2] Some striking examples of short period gravity waves have been reported [e.g., *Taylor et al.*, 1995; *Smith et al.*, 2003, 2005; *Brown et al.*, 2004; *She et al.*, 2004] which exhibit distinct features beyond those predicted by linear theory. Consistent with waves near the ducted/evanescent limit of propagation, these waves have typical observed periods of $\tau \sim$ 5 min and horizontal wavelengths $\lambda_x \sim$ 20 km. The events appear front-like, exhibiting a distinct leading edge, and are usually accompanied by a set of high contrast short-period wave perturbations in the background airglow emission intensity, where the short period event is apparently phase locked with a background intensity transition. In each of the reports cited above, different airglow layers appear to emit in opposite phase relative to other layers, such that the phase difference between OH and OI emissions, for example, is 180° [e.g., *Taylor et al.*, 1995; *Snively and Pasko*, 2005, and references cited therein].

[3] Theories presented to explain this type of event, first observed during the ALOHA93 campaign and reported by *Taylor et al.* [1995], have assumed that the wave was vertically trapped. *Munasinghe et al.* [1998] proposed that the wave satisfied a fully ducted wave mode solution arising

from atmospheric thermal structure. By this explanation, the phase reversals of airglow intensity may arise from a waveguide node (phase reversal) present between airglow layers; the front-like intensity jump, however, is not easily explained. Alternatively, *Dewan and Picard* [1998] suggested that the wave was consistent with an internal bore propagating in a thermal inversion layer [e.g., *Meriwether and Gerrard*, 2004, and references therein], with the airglow layers perturbed in opposite directions by upward and downward oscillations trailing the initial front. In both of these explanations, the airglow phase differences are assumed to arise from ducted waves with dynamic phase reversals (nodes) at distinct altitudes between emission layers.

[4] Because of their very short periods, such waves are typically evanescent throughout much of the mesosphere. It is thus improbable that they could have propagated directly from a tropospheric source, suggesting that such waves are likely generated in situ. Proposed in situ wave generation mechanisms include those associated with nonlinear resonant excitation by other short period waves [e.g., *Chimonas et al.*, 1996; *Snively and Pasko*, 2003], linear body forcing associated with wave breaking [e.g., *Vadas et al.*, 2003], or internal bore formation due to gravity wave critical layer phenomena or large-scale wave breaking [e.g., *Dewan and Picard*, 2001; *Smith et al.*, 2005; *Seyler*, 2005].

[5] Recent numerical model results lend conflicting insight. *Seyler* [2005] demonstrated bore formation due to gravity wave breaking in a specialized numerical model. Two long-period waves, one propagating upward and another downward, were arranged to meet in the center of the simulation domain where a thermal duct was present. Their combined perturbations resulted in wave breaking and

[1]Communications and Space Sciences Laboratory, Department of Electrical Engineering, Pennsylvania State University, University Park, Pennsylvania, USA.
[2]Center for Atmospheric and Space Sciences and Physics Department, Utah State University, Logan, Utah, USA.
[3]Department of Physics and Astronomy, University of Western Ontario, London, Ontario, Canada.
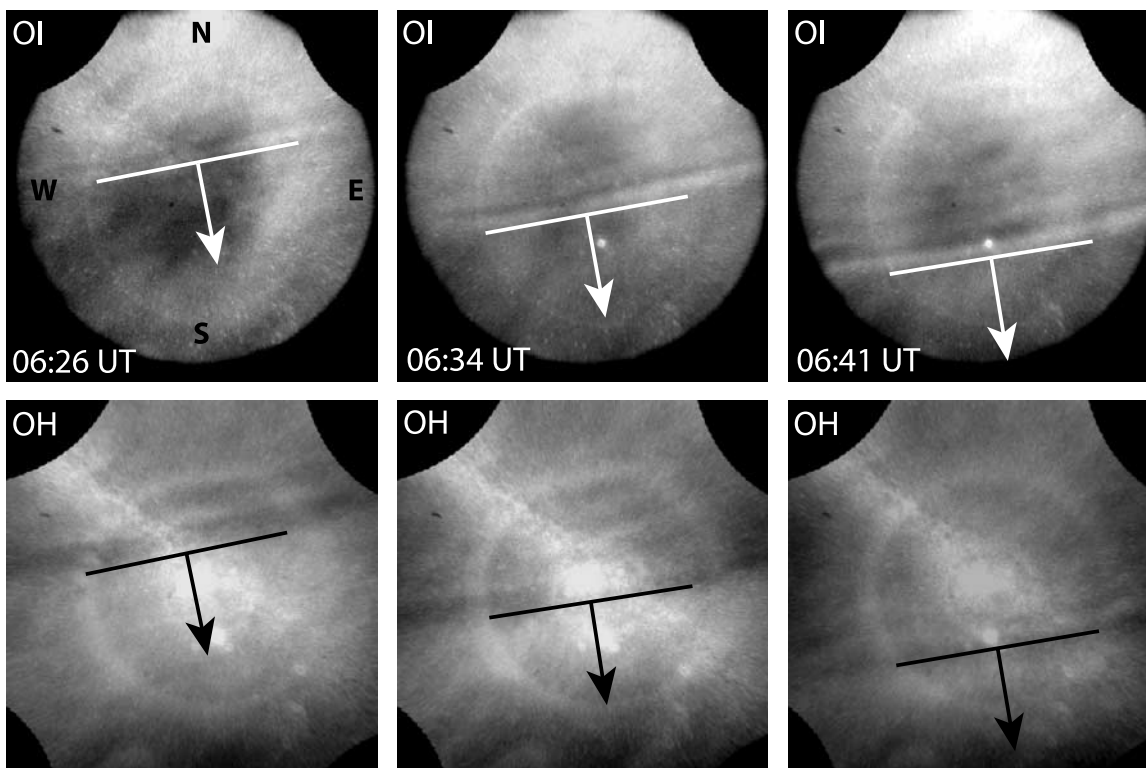
Figure 1. OH and OI airglow images depicting short-period wave propagation with opposite intensity emissions for the wave perturbation and for the "front-like" background enhancement.

the nonlinear excitation of ducted waves. It was noted that only ducted waves satisfying odd modes (thereby excluding the excitation of zero- or two-node waves) could be excited under the specified conditions. This implies that ducted waves generated by this mechanism would necessarily have a phase reversal (node) present in the solution for vertical fluid perturbation velocity. *Snively and Pasko* [2005] simulated ducted wave excitation, and resulting airglow modulation, of a two-node wave consistent with *Munasinghe et al.*'s [1998] explanation of the spectacular event reported by *Taylor et al.* [1995]. However, it was shown that the modeled ducted wave structure did not lead to nodes between airglow layers (although nodes were present at higher altitudes); instead the differing responses of OH and OI airglow emissions led to a 180° phase difference between the emissions. By this explanation, airglow photochemistry alone leads to a 180° phase shift, without the need for a wave phase reversal between the altitudes of the OH and OI airglow layers.

[6] Concerning the ducting mechanism, *Dewan and Picard* [2001] assumed that temperature inversion layers arising from large-scale atmospheric waves provide the stable thermal duct in which a bore (or other small-scale ducted waves) may propagate. The formation of temperature inversion layers by gravity wave critical layer phenomena and by tidal wave structure has been studied by, e.g., *Huang et al.* [1998] and *Picard et al.* [2004], respectively. In their analysis, *Snively and Pasko* [2005] assumed a combination of thermal and wind structure in modeling a ducted wave resembling that observed during the ALOHA93 campaign [*Taylor et al.*, 1995]. Other studies utilizing radar wind data together with airglow imaging data have found Doppler ducting to be a relevant process at mesopause heights [*Isler*

et al., 1997]. The possibility that a front-like event resembling those previously reported [e.g., *Taylor et al.*, 1995; *Smith et al.*, 2003; *Brown et al.*, 2004] may be ducted by a strong wind peak rather than by thermal structure has not been explored. Additionally, correlation with tidal perturbations has not been previously confirmed.

[7] In this paper we present new measurements and modeling of a front- like wave event recorded using an all-sky CCD imager together with meteor wind radar observations using a SKiYMET radar both located at Bear Lake Observatory, Utah [*Hocking et al.*, 2001]. During this event a large-scale oscillation, likely associated with a semidiurnal tide, was observed to dominate the wind field throughout the night and the previous day. This tide created a strong localized peak in the background wind which was sufficient to Doppler duct the observed short-period wave motion. Excitation of short-period ducted waves is simulated in a model atmosphere, along with resulting OH and OI airglow intensity modulation. Data and model results are then compared with similar previously reported events.

2. Data and Analysis

[8] At 0630 UT on 29 November 2000 a well-defined short-period wave event was observed by the Utah State University all-sky imager located at Bear Lake Observatory (BLO) together with a colocated University of Western Ontario meteor radar. The wave, visible in both OH and OI emissions is depicted in Figure 1. The OH and OI emissions typically arise at ~87 and ~96 km altitude, respectively [e.g., *Taylor et al.*, 1995]. The OH emission data was broadband filtered with a passband of 710–
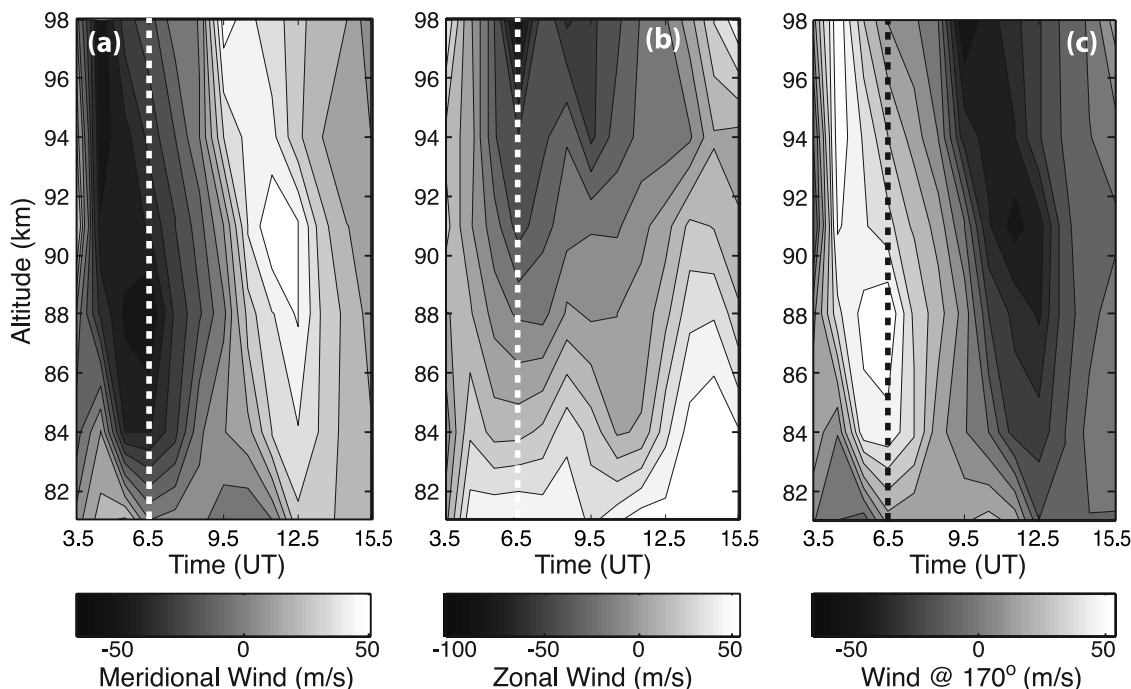
Figure 2. Wind velocity measurements taken on site at Bear Lake Observatory (BLO) depicting flow projected along the (a) meridional direction, (b) zonal direction, and (c) direction of short-period wave propagation, spanning a 12-hour duration from 0330 to 1530 UT. Black and white lines parallel to leading phase fronts are placed at the same relative positions in each plot.

930 nm, with a notch at 865 nm to remove the O2(0,1) contribution. The event was determined to have a horizontal wavelength (λ_x) of $\simeq 22$ km and phase velocity (v_p) of $\simeq 75$ m/s, remarkably similar to the ALOHA93 frontal event first reported by *Taylor et al.* [1995]. Direction of wave propagation was aligned toward the SSE (170° from north). As with previously reported observations, a conspicuous phase shift between OH and OI emission structures was present in addition to a sharp "step-like" change in the background intensity locked to the leading edge of the event.

[9] Figures 2a and 2b depicts comparison of meridional and zonal wind data, respectively, for 29 November 2000, spanning from 0330 UT to 1530 UT. The wind data clearly exhibit a 12-hour periodicity, consistent with a semidiurnal tide. Figure 2c illustrates wind data spanning 12 hours from 0330 UT through 1530 UT, 29 November 2000, where the dashed line denotes 0630 UT, the time of the observed wave event. This wind flow is presented along the direction of short-period wave propagation (170° from North). Figure 3 depicts comparison of meridional wind data for 28 and 29 November 2000, taken at 88 km altitude. Observed dynamic wind structures were quite consistent with a semidiurnal, 12-hour tidal oscillation present for the duration of the night and previous day.

[10] Figure 4a depicts wind velocity at 0630 UT projected along the direction of short-period wave propagation. An analytical wave-like wind structure is plotted (dashed line), which is used for the model run presented in section 3. The model wind is given analytically by $u = 100$ m/s · [sech((z − 106 km)/17) sin(−2π(z − 98 km)/40 km)]. A semidiurnal vertical wavelength of 40 km is assumed on the basis of wind data and previous observations of tides [e.g., *Zhang et*

al., 2003]. Also plotted (solid line) is an HWM 93 model wind profile calculated for the time (0630 UT), date (29 November 2000), and location (Bear Lake Observatory, 41.6°N, 111.6°W) of observation [*Hedin et al.*, 1991], which has been multiplied by a factor of 3 to compensate for the significantly greater observed magnitude. Wind flow velocity along the direction of short period wave propagation was near a nightly maximum (>60 m/s at 88 km) at the time of wave occurrence. The problem of wave ducting upon a spatially periodic background wind field has been
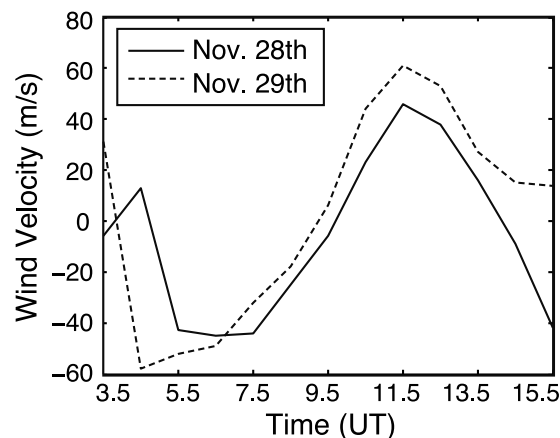

Figure 3. Meridional wind velocity at 88 km altitude, measured on site at BLO spanning a 12-hour duration from 0330 to 1530 UT for 28 and 29 November 2000, clearly illustrating semidiurnal wind periodicity. Positive values indicate northward winds.
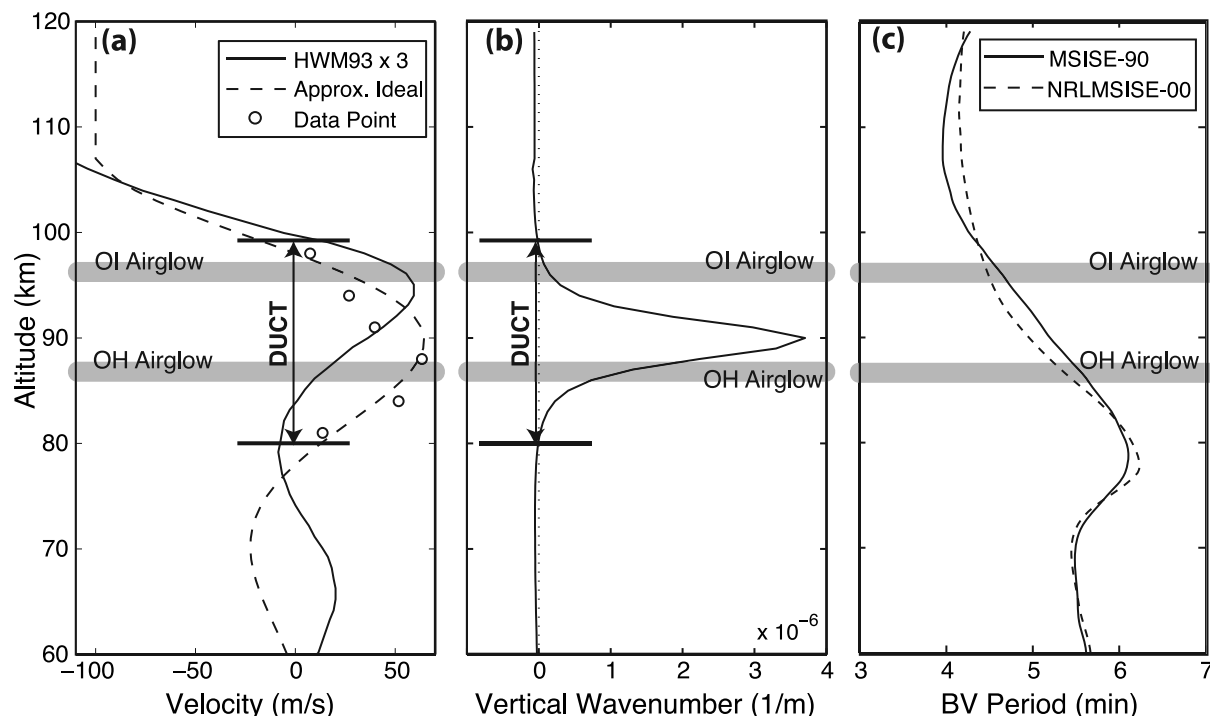
Figure 4. (a) Wind velocity along the direction of wave propagation (see text for details). (b) Vertical wave number squared (k_z^2) for the Taylor-Goldstein equation plotted, showing robust duct structure present throughout the airglow region given the parameters of the observed wave. (c) Brunt-Väisälä period profile calculated from MSISE-90 and NRLMSISE-00 model data.

explored as a wave-wave interaction [e.g., *Liu*, 1970] and is analogous to Doppler ducting on a wind peak [e.g., *Isler et al.*, 1997].

[11] Figure 4b depicts the vertical wave number "squared" of the Taylor-Goldstein equation (k_z^2) [e.g., *Isler et al.*, 1997] given the properties of the observed wave, the model wind profile in Figure 4a, and an MSISE-90 model atmospheric profile [*Hedin*, 1991]. The Brunt-Väisälä period for the model profile is plotted in Figure 4c and is shown for MSISE-90 and NRLMSISE-00 models [*Hedin*, 1991; *Picone et al.*, 2002]; Brunt-Väisälä period of the ducting region is ~5 min. The strong wind structure alone is able to support ducted short-period wave propagation. We cannot model the actual thermal structure associated with the observed large-scale wave background, as no measured data are available, and typical model results reproduce much weaker tidal perturbations than those observed [*Zhang et al.*, 2003]; implications of this assumption will be described in section 4. The vertical wave number of the ducted wave approaches zero (reflection) at altitudes just above the OI airglow layer and just below the OH airglow layer. The ground-relative period of the observed wave was ~4.9 min. The intrinsic period, assuming ~40 m/s average flow at both airglow layer peak altitudes, was ~10.5 min, but varies significantly with altitude because of the wind flow.

[12] The analytical model wind profile artificially fixes the flow velocity at −100 m/s above 106 km, to guarantee that wave energy will be reflected or dissipated before reaching the domain boundary. If wind structure were to permit propagation above 100 km, the duct would extend vertically into the lower thermosphere [e.g., *Snively and Pasko*, 2005]. Although wind data are not available above

100 km or below 80 km, we have assumed that this strong wind flow of opposite phase likely exists (above and below), consistent with observed wave-like wind structure and downward tidal phase progression measured over the night of the event and previous 24 hours, and with HWM 93 wind model data presented. Even if wind flow just below the lowest data point became slightly faster in the direction of short-period wave propagation, the model Doppler duct boundary will remain, but occur at a slightly lower altitude because of reduced stability near mesopause (Figure 4c). In fact, the highest and lowest points of the data set coincide very closely with the predicted duct boundaries, suggesting that actual upper and lower boundaries of the duct likely existed near these altitudes. It is unlikely that the wave could have propagated freely from a tropospheric source, because of its very short ground-relative period. Only in the case of significant wind flow along the direction of wave propagation, from tropopause to mesopause, would it be possible for a wave with such short period to avoid evanescence and propagate directly to airglow altitudes. It remains possible, however, that a lower duct was present from which the observed wave could have tunneled [e.g., *Fritts and Yuan*, 1989].

[13] The possibility that this wave may have been ducted by Doppler shift is contrary to assumptions made in recent interpretations of the ALOHA93 event first reported by *Taylor et al.* [1995], where thermal variations and weak wind flow have been assumed to form the duct [e.g., *Munasinghe et al.*, 1998; *Dewan and Picard*, 1998; *Snively and Pasko*, 2005]. Given the strong background flow and the short ground-relative period of the observed ducted wave, it is unlikely that this wave propagated vertically
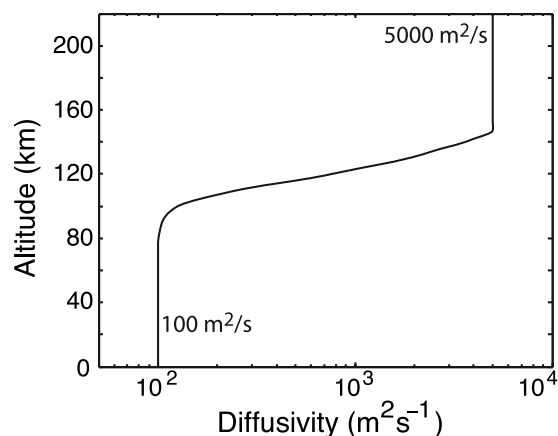
Figure 5. Model diffusivity profiles for kinematic viscosity, including approximate eddy diffusion and molecular diffusion effects.

from a tropospheric source to its point of observation, suggesting in situ generation. Unfortunately, evidence does not rule out, or favor, any individual mechanism discussed in section 1. Whether the semidiurnal tide played a role in the generation of the short-period wave, or whether it merely formed a preferential ducting region, is uncertain. Thus, rather than modeling a physical generation mechanism, we will model the excitation of ducted waves using an idealized in situ source, as a means to study their vertical mode structure, propagation characteristics, and interaction with OH and OI airglow photochemistry.

3. Numerical Model

[14] Numerical simulation results are obtained with the model presented by *Snively and Pasko* [2003, 2005] and calculated using the CLAWPACK software package (http://www.amath.washington.edu/~claw) [*LeVeque*, 2002]. Background atmospheric conditions are as described in section 2, using the analytic model wind profile depicted in Figure 4a. The present version of the numerical model does not use sponge layers or artificial damping; instead, increasing molecular kinematic viscosity is used to naturally damp waves that propagate vertically toward the upper boundary. At lower altitudes (below ~110 km), the kinematic viscosity is fixed at a value which is comparable or slightly greater than measured eddy diffusion throughout the middle atmosphere (100 m^2 s^{-1}) [e.g., *Hocking*, 1990; *Fukao et al.*, 1994]. At altitudes above those where eddy diffusion dominates, the diffusion coefficient is dominated by the molecular kinematic viscosity, which is estimated by assuming that it is inversely proportional to the decreasing atmospheric density [*Gossard and Hooke*, 1975, p. 222]. Maximum total kinematic viscosity is restricted to 5000 m^2 s^{-1} to reduce numerical error arising from the high-altitude source; this transition occurs well above the altitude of the ducted wave, and does not affect the solution below ~150 km. Figure 5 depicts the model viscosity profile. At mesopause altitudes, however, total diffusion remains relatively weak and does not strongly affect the solution.

[15] Airglow models for OH(8,3) and OI 557.7 nm emissions, which are employed in the present study, are identical to those used by *Snively and Pasko* [2005], yielding vertically integrated photon emission rates. Although only one transition of the OH(v = 8) vibrational state is calculated, states v = 6–9 are excited via the same reaction, albeit in different quantities. The OH(8,3) emission yields a characteristic wavelength of 724.3 nm, and thus would have been passed by the filter used in the BLO airglow imager. The OH photon emission rates are calculated using simple time-dependent ozone chemistry and transport, while the OI is calculated using a steady state approximation with atomic oxygen transport [*Snively and Pasko*, 2005, and references therein]. For the specified MSISE-90 profiles, the OH(8,3) Meinel emission peaks at a rather high altitude of ~89 km, while the OI emission peaks at 96 km. The actual heights of the emission layers were not measured on this occasion.

[16] The source of the gravity waves is positioned at x_o = 400 km and z_o = 90 km (i.e., 400 km from the left boundary of the simulation domain and at 90 km altitude). It is a mechanical traveling wave oscillator providing a vertical force at a chosen frequency (ω) and horizontal wave number (k_x) of the form $\sim\exp[-(x-x_o)^2/2\sigma_x^2 - (z-z_o)^2/2\sigma_z^2 - (t-t_o)^2/2\sigma_t^2] \cos[\omega t - k_x(x-x_o) - k_z(z-z_o)]$, where σ_x and σ_z are the Gaussian envelope's horizontal and vertical half widths, respectively, and σ_t is the temporal Gaussian half width; the position given by x_o, z_o, and t_o corresponds to the source maximum in space and time. The source is specified by ground-relative parameters ω = 0.0214 rad/sec (T = 4.9 min), k_x = 0.0002856 rad/m (λ_x = 22 km), k_z = 0 or 0.000419 rad/m (λ_x = ∞ or ≃15 km), σ_x = 30 km, σ_z = 3 km, and σ_t = 16.67 min (1000 sec).

4. Results and Discussion

[17] Figure 6a depicts a single frame from the numerical model taken at t = 3000 s; here, the source has zero nodes in the vertical velocity field (source k_z = 0). The zero-node wave (having no phase reversals of vertical velocity along the z direction) was excited linearly by an artificial wave source situated inside the duct, and has approximate ground-relative phase velocity v_p ∼ 100 m/s and λ_x ≃ 22 km at the airglow layer peaks. The one-node wave (having one phase reversal of vertical velocity along the z direction) that is visible trailing the zero-node wave is also a product of the same source, and has v_p ∼ 75 m/s but λ_x ∼ 30 km at the OI peak and λ_x < 22 km at the OH peak. Additional modes and spectral components are visibly propagating simultaneous with the one-node wave. The Doppler duct fully traps the waves, allowing them to travel horizontally through the mesopause airglow region. As predicted analytically in section 2, ducted wave propagation in the numerical model is restricted to 80–98 km. The number of simulated wave crests of the zero-node and multinode modes is determined arbitrarily by the duration of forcing and by the spatial structure of the artificial source.

[18] Figure 6b depicts a single frame from the numerical model taken at t = 4500 s; here, the source has two nodes in the vertical velocity field (source k_z = 0.000419 rad/m). The excited ducted wave, while more complex in structure, satisfies a ducted wave mode with ground-relative phase velocity v_p ∼ 80 m/s. While the ALOHA93 event is believed to have been a two-node thermally ducted wave
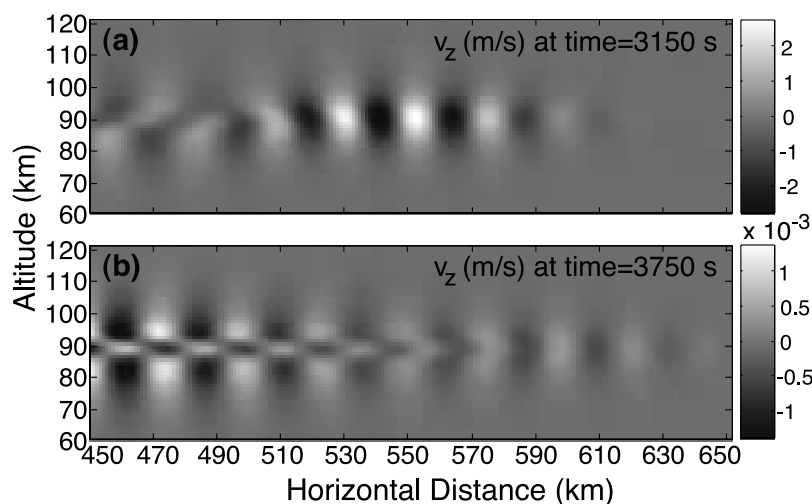
Figure 6. Model results for scaled vertical fluid velocity field depicting (a) excited zero-node ducted wave, propagating in the Doppler duct and trailed by slower one-node ducted wave, and (b) excited two-node wave following a zero-node wave dispersed from the Gaussian packet excited by the source. Vertical velocity field is scaled by a factor of $(\rho/\rho_o)^{1/2}$.

propagating in a thick region above mesopause [*Snively and Pasko*, 2005], the observed Doppler duct for the event discussed in the present paper is confined entirely in the airglow region.

[19] These wave packets agree with modes excited by the Gaussian forcing; the modeled waves have propagated a distance of ∼200 km, and packet has dispersed significantly. The zero-node mode propagates fastest and appears prior to multinode modes. It is important to note that because of the dispersion properties of the Doppler duct, the zero-node wave has higher group velocity than the multinode waves. This is in contrast to typical thermal duct dispersion and arises because of the group and phase velocity dependence on wind speed; the zero-node wave is spatially confined to the fastest region of the wind peak, and its group and phase velocities are strongly determined by the wind velocity.

[20] The vertical structures of the modeled ducted waves are partly determined by assumptions outlined in section 2; most importantly, that we do not model actual background thermal structure arising because of the large-scale tidal motion. Strong thermal perturbations would certainly accompany the observed wind profile [e.g., *Li et al.*, 2005]. While the duct itself arises primarily from Doppler shift, this tidal thermal background would additionally affect ducted wave propagation via its effects on the Brunt-Väisälä profile, modifying the vertical structure and dispersion properties of the ducted waves. We note that both modeled zero-node and multinode waves have phase velocities or wavelengths greater than those observed. Modification of duct shape and thickness, and resulting Brunt Väisälä frequency profiles due to tidal thermal effects likely contributes to this discrepancy. For example, if the tide was acting to reduce atmospheric stability, thereby increasing the Brunt Väisälä period, the intrinsic phase velocities of the zero-node mode would be reduced. Additionally, reduction in duct thickness would allow waves of longer intrinsic period (lower intrinsic frequency and phase velocity) to satisfy low-order wave modes of the same horizontal wavelength. This problem is complicated significantly,

however, by the sharp wind variations inside and around the duct. For example, wave energy concentrated in the center of the wind peak will experience a stronger Doppler shift than a wave spread out above or below the peak. It is this effect that leads to the fast propagation of the zero-node wave compared to multinode waves. While the duct itself is robust, the modal properties of the duct may vary dramatically with slight changes in atmospheric conditions. Future theoretical and modeling studies of short-period wave ducting in large-scale, large-magnitude wave structures may help to elucidate these effects.

[21] Figure 7a depicts the corresponding vertically integrated airglow emissions due to the modeled zero-node gravity wave in Figure 6a. The nearly 180° phase difference between emission intensities agrees with the airglow observations in Figure 1. This is also consistent with numerical results presented by *Snively and Pasko* [2005], where a 180° phase difference between OH(8,3) and OI airglow emissions was found for a modeled wave similar to that reported by *Taylor et al.* [1995]. Related observations reviewed in section 1 also exhibit this feature, although many interpretations, also reviewed in section 1, attribute the opposite intensities to arise from opposite wave dynamics, rather than opposite photochemical responses. This phase shift arises from the temperature and time dependence of OH and OI airglow emission chemistry, rather than from differences in wave dynamic phase at the two airglow layers. Specifically, the reaction leading to production of vibrationally excited OH occurs on a relatively slow time-scale; the chemical lifetime of ozone, consumed by this OH production reaction, is on the order of a gravity wave period [e.g., *Snively and Pasko*, 2005, and references therein]. Therefore the OH emission process becomes controlled and rate limited by OH production. This is contrary to the case of the OI emission, where chemical time dependence is insignificant on gravity wave scales, and also contrary to the behavior of the OH emission response to gravity waves with longer periods over 15 min [e.g., *Swenson and Gardner*, 1998].
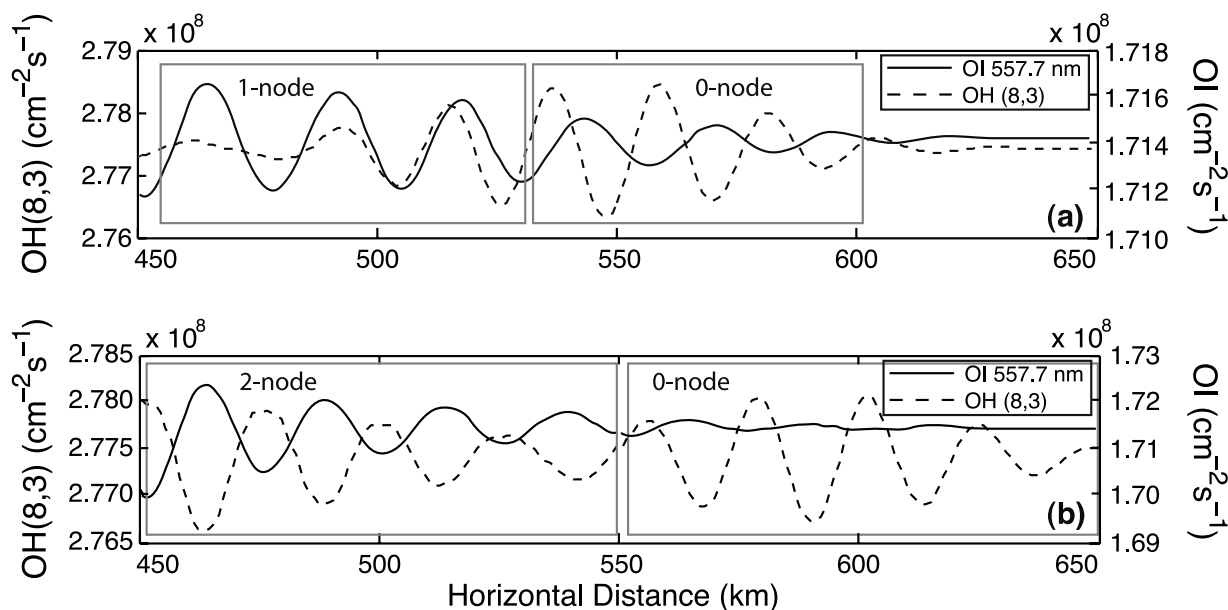
Figure 7. Model-generated vertically integrated photon emission rates for OH(8,3) (~89 km) and OI (~95 km) airglow intensities for (a) zero-node and one-node waves and (b) zero-node and two-node waves. A ~180° phase difference between OH and OI intensities is observed for zero- and two-node waves, while a ~0° phase difference is observed for the one-node wave [*Snively and Pasko*, 2005].

[22] Figure 7b depicts the vertically integrated airglow emissions due to the two-node gravity wave in Figure 6b. Here, the phase velocity of the wave is ≃80 m/s, which is closer to that observed. However, the wave is still preceded by a zero-node wave generated by the Gaussian source. It is notable that, although the phase velocity of the modeled zero-node wave is higher than the observed wave, the airglow phasing effects are still observed for the two-node 80 m/s wave; the solution is similar to the thermally ducted wave studied by *Snively and Pasko* [2005].

[23] The zero-node wave here propagates fastest and precedes other ducted wave modes with more complex structure. It is most able to produce a clear airglow signature, as its polarization properties lead to strong vertical fluid perturbations, and its lack of vertical phase reversals prevents cancellation effects because of the vertical integration of airglow emissions. This also enforces that the wave will perturb each airglow layer with identical phase. Under certain conditions, multinode ducted waves are able to perturb both airglow layers with the same phase where vertical wavelengths become very long [e.g., *Snively and Pasko*, 2005]. However, the observed duct is sufficiently narrow, confining waves to the airglow region, such that vertically integrated emissions are significantly affected by wave dynamic phase. The one-node wave leads to in-phase OH and OI intensity perturbations, as its dynamical phase reversal negates the effects of the photochemical phase reversal. Variations of wind flow, and consequent Doppler shift, with altitude also result in distortions in the integrated wave structure, particularly for the multinode waves which span a wider region of space.

[24] One feature lacking from the model results is the apparent background intensity change associated with the passage of the short period wave, as discussed in section 2 and seen in Figure 1. It remains unclear whether the observed intensity jump was a feature of the large-scale atmospheric background, or if it was associated with the propagation or generation of the short period wave. An interesting feature of the reported event is that the short-period wave was ducted near a nightly maximum in tidal wind velocities along the direction of short-period wave propagation for the duration of the night (Figure 2). Phase of tidal temperature and vertical fluid velocity perturbations associated with tides are shifted over latitude [e.g., *Hagan et al.*, 2001], allowing the possibility that the event occurred at a tidal phase transition of temperature and vertical fluid velocity, perhaps leading to background transitions in OH and OI emission intensity due to the large magnitude of the tides. Tides are known to modulate airglow intensity, and can result in large-scale perturbations of OH and OI airglow that emit in opposite phase; this phasing effect has been reported for the diurnal tide by *Zhang and Shepherd* [1999]. However, it seems unlikely that tidal airglow modulation could lead to the sharpness of OH and OI background intensity transients observed simultaneous with the short-period wave event.

[25] It is important to note that this event also resembles a "wall" wave as reported by *Swenson and Espy* [1995] and *Swenson et al.* [1998], due to the large-scale airglow modulation simultaneous to the small-scale event. Such an event could contribute to the observed background intensity changes. However, the waves described by *Swenson and Espy* [1995] and *Swenson et al.* [1998] have periods on the order of 1 hour; since the meteor radar data are provided at hourly intervals, averaged over space and time, they are not sensitive to wave motions with periods on the order of 2 hours or less.

[26] Chemical explanations for background intensity changes accompanying propagation of strong short-period gravity waves also exist. It has been suggested that secular

variations of atomic oxygen and other minor species densities may lead to enhancements or depletions of airglow intensity in conjunction with the propagation of a gravity wave packet [e.g., *Hickey and Walterscheid*, 2001]; but it is not known if such effects could resemble the intensity change observed here, and the modeled waves here do not produce significant secular changes of intensity.

[27] Theories of internal bore formation resulting from steepening, breaking, or instability of large-scale gravity waves may also play a role in explaining background intensity modulation and short period in situ wave generation [e.g., *Seyler*, 2005; *Smith et al.*, 2005]. While the horizontal wind maximum may imply conditions favorable for bore formation due to wave steepening and instability, conditions are also favorable for ducting of waves generated via any other mechanism.

5. Conclusions

[28] A ducted wave event has been reported and modeled, which strongly resembles past reported observations by *Taylor et al.* [1995], *Brown et al.* [2004], and *Smith et al.* [2003, 2005] of front-like wave perturbations. Airglow images depict a short-period gravity wave with period $\tau \sim 4.9$ min and wavelength $\lambda_x \sim 22$ km. It is notable that OH and OI airglow images appear with opposite phase intensity, both in the short-period wave perturbations and in a background intensity "step" which appears phase locked to the leading edge front. Meteor wind data captured over the 1-hour duration of the event suggest that the event occurred during a nightly peak of wind velocity, likely associated with the semidiurnal tide. The observed tidal wind structure created favorable conditions for Doppler ducting of the short-period wave, without the explicit need for a thermal inversion layer.

[29] The modeled short-period wave's OH and OI airglow intensity perturbations appear nearly $180°$ out of phase, due to time and temperature dependence of OH and OI chemistry, consistent with results of *Snively and Pasko* [2005]. Phase velocities of modeled ducted zero-node waves are higher than those observed, suggesting that actual tidal structure of wind and temperature was significant in determining observed wave properties, or that multiple-node wave structure was present. Furthermore, the observed intensity jump is not reproduced given the presently modeled scenario. While the peak of meridional wind flow may imply transitions of tidal temperature and vertical winds, possibly leading to simultaneous and opposite changes in OH and OI background intensity [e.g., *Zhang and Shepherd*, 1999], it is unclear if this could account for the sharp frontal structure observed. Alternative theories for the intensity jump include secular variations of airglow intensity due to short period wave propagation [e.g., *Hickey and Walterscheid*, 2001], internal bore formation [e.g., *Seyler*, 2005], or the simultaneous presence of a large-scale upward propagating wave [e.g., *Swenson and Espy*, 1995]. With the absence of temperature data for this event, future studies will be necessary to explore these and other possibilities.

References

Brown, L. B., A. J. Gerrard, J. W. Meriwether, and J. J. Makela (2004), All-sky imaging observations of mesospheric fronts in OI 557.7 nm and broadband OH airglow emissions: Analysis of frontal structure, atmospheric background conditions, and potential sourcing mechanisms, *J. Geophys. Res.*, *109*, D19104, doi:10.1029/2003JD004223.

Chimonas, G., H. M. Hauser, and R. D. Bennett (1996), The excitation of ducted modes by passing internal waves, *Phys. Fluids*, *8*(6), 1486–1505.

Dewan, E. M., and R. H. Picard (1998), Mesospheric bores, *J. Geophys. Res.*, *103*, 6295–6305.

Dewan, E. M., and R. H. Picard (2001), On the origin of mesospheric bores, *J. Geophys. Res.*, *106*(D3), 2921–2928.

Fritts, D. C., and L. Yuan (1989), An analysis of gravity wave ducting in the atmosphere: Eckart's resonances in thermal and doppler ducts, *J. Geophys. Res.*, *94*(D15), 18,455–18,466.

Fukao, S., M. D. Yamanaka, N. Ao, W. K. Hocking, T. Sato, M. Yamamoto, T. Tsuda, and S. Kato (1994), Seasonal variability of vertical eddy diffusivity in the middle atmosphere: 1. Three-year observations by the middle and upper atmosphere radar, *J. Geophys. Res.*, *99*, 18,973–18,987.

Gossard, E. E., and W. H. Hooke (1975), *Waves in the Atmosphere*, Elsevier, New York.

Hagan, M. E., R. G. Roble, and J. Hackney (2001), Migrating thermospheric tides, *J. Geophys. Res.*, *106*, 12,739–12,752.

Hedin, A. E. (1991), Extension of the MSIS thermospheric model into the middle and lower atmosphere, *J. Geophys. Res.*, *96*, 1159–1172.

Hedin, A. E., N. W. Spencer, M. A. Biondi, R. G. Burnside, G. Hernandez, and R. M. Johnson (1991), Revised global model of thermosphere winds using satellite and ground-based observation, *J. Geophys. Res.*, *96*, 7657–7688.

Hickey, M. P., and R. L. Walterscheid (2001), Secular variations of OI 5577 Å airglow in the mesopause region induced by transient gravity wave packets, *Geophys. Res. Lett.*, *28*(4), 701–704.

Hocking, W. K. (1990), Turbulence in the region 80–120 km, *Adv. Space Res.*, *10*(12), 153–161.

Hocking, W. K., B. Fuller, and B. Vandepeer (2001), Real-time determination of meteor-related parameters utilizing modern digital technology, *J. Atmos. Sol. Terr. Phys.*, *63*, 155–169.

Huang, T. Y., H. Hur, T. F. Tuan, X. Li, E. M. Dewan, and R. H. Picard (1998), Sudden narrow temperature-inversion-layer formation in ALOHA-93 as a critical-layer-interaction phenomenon, *J. Geophys. Res.*, *103*, 6323–6332.

Isler, J. R., M. J. Taylor, and D. C. Fritts (1997), Observational evidence of wave ducting and evanescence in the mesosphere, *J. Geophys. Res.*, *102*, 26,301–26,313.

LeVeque, R. J. (2002), *Finite Volume Methods for Hyperbolic Problems*, Cambridge Univ. Press, New York.

Li, F., A. Z. Liu, and G. R. Swenson (2005), Characteristics of instabilities in the mesopause region over Maui, Hawaii, *J. Geophys. Res.*, *110*, D09S12, doi:10.1029/2004JD005097.

Liu, C. H. (1970), Ducting of acoustic-gravity waves in the atmosphere with spatially periodic wind shears, *J. Geophys. Res.*, *75*, 1339–1341.

Meriwether, J. W., and A. J. Gerrard (2004), Mesosphere inversion layers and stratosphere temperature enhancements, *Rev. Geophys.*, *42*, RG3003, doi:10.1029/2003RG000133.

Munasinghe, G., H. Hur, T. Y. Huang, A. Bhattachryya, and T. F. Tuan (1998), Application of the dispersion formula to long- and short-period gravity waves: Comparisons with ALOHA-93 data and an analytical model, *J. Geophys. Res.*, *103*, 6467–6481.

Picard, R. H., P. P. Wintersteiner, R. R. Winick, C. J. Mertens, M. G. Mlynczak, J. M. Russell III, L. L. Gordley, W. E. Ward, C. Y. She, and R. R. O'Neil (2004), Tidal and layer structure in the mesosphere and lower thermosphere from TIMED/SABER CO_2 15-μm emission, in *Remote Sensing of Clouds and the Atmosphere IX*, edited by A. Comeron et al., *Proc. SPIE Int. Soc. Opt. Eng.*, *5571*, 182–192, doi:10.1117/12.568060.

Picone, J. M., A. E. Hedin, D. P. Drob, and A. C. Aikin (2002), NRLMSISE-00 empirical model of the atmosphere: Statistical comparisons and scientific issues, *J. Geophys. Res.*, *107*(A12), 1468, doi:10.1029/2002JA009430.

Seyler, C. E. (2005), Internal waves and undular bores in mesospheric inversion layers, *J. Geophys. Res.*, *110*, D09S05, doi:10.1029/2004JD004685.

She, C. Y., T. Li, B. P. Williams, T. Yuan, and R. H. Picard (2004), Concurrent OH imager and sodium temperature/wind lidar observation of a

mesopause region undular bore event over Fort Collins/Platteville, Colorado, *J. Geophys. Res.*, *109*, D22107, doi:10.1029/2004JD004742.

Smith, S. M., M. J. Taylor, G. R. Swenson, C. She, W. Hocking, J. Baumgardner, and M. Mendillo (2003), A multidiagnostic investigation of the mesospheric bore phenomenon, *J. Geophys. Res.*, *108*(A2), 1083, doi:10.1029/2002JA009500.

Smith, S. M., J. Friedman, S. Raizada, C. Tepley, J. Baumgardner, and M. Mendillo (2005), Evidence of mesospheric bore formation from a breaking gravity wave event: Simultaneous imaging and lidar measurements, *J. Atmos. Sol. Terr. Phys.*, *67*(4), 345–356, doi:10.1016/j.jastp.2004.11.008.

Snively, J. B., and V. P. Pasko (2003), Breaking of thunderstorm-generated gravity waves as a source of short-period ducted waves at mesopause altitudes, *Geophys. Res. Lett.*, *30*(24), 2254, doi:10.1029/2003GL018436.

Snively, J. B., and V. P. Pasko (2005), Antiphase OH and OI airglow emissions induced by a short-period ducted gravity wave, *Geophys. Res. Lett.*, *32*, L08808, doi:10.1029/2004GL022221.

Swenson, G. R., and P. J. Espy (1995), Observations of 2-dimensional airglow structure and Na density from the ALOHA, October 9, 1993 "storm flight," *Geophys. Res. Lett.*, *22*(20), 2845–2848.

Swenson, G. R., and C. S. Gardner (1998), Analytical models for the response of the mesospheric OH* and Na layers to atmospheric gravity waves, *J. Geophys. Res.*, *103*, 6271–6294.

Swenson, G. R., J. Qian, J. M. C. Plane, P. J. Espy, M. J. Taylor, D. N. Turnbull, and R. P. Lowe (1998), Dynamical and chemical aspects of the mesospheric Na "wall" event on October 9, 1993 during the Airborne Lidar and Observations of Hawaiian Airglow (ALOHA) campaign, *J. Geophys. Res.*, *103*(D6), 6361–6380.

Taylor, M. J., D. N. Turnbull, and R. P. Lowe (1995), Spectrometric and imaging measurements of a spectacular gravity wave event observed during the ALOHA-93 campaign, *Geophys. Res. Lett.*, *22*(20), 2849–2852.

Vadas, S. L., D. C. Fritts, and M. J. Alexander (2003), Mechanism for the generation of secondary waves in wave breaking regions, *J. Atmos. Sci.*, *60*, 194–214.

Zhang, S. P., and G. G. Shepherd (1999), The influence of the diurnal tide on the O(^{1}S) and OH emission rates observed by WINDII on UARS, *Geophys. Res. Lett.*, *26*(4), 529–532.

Zhang, S. P., L. P. Goncharenko, J. E. Salah, R. G. Roble, and G. G. Shepherd (2003), Climatology of neutral winds in the lower thermosphere over Millstone Hill (42.6°N) observed from ground and from space, *J. Geophys. Res.*, *108*(A1), 1051, doi:10.1029/2002JA009512.

_____

W. K. Hocking, Department of Physics and Astronomy, University of Western Ontario, 1151 Richmond St. North, London, ON, Canada N6A 3K7.

V. P. Pasko and J. B. Snively, CSSL, Department of Electrical Engineering, Pennsylvania State University, 211B Electrical Engineering East, University Park, PA 16802, USA. (vpasko@psu.edu; jbs231@psu.edu)

M. J. Taylor, Center for Atmospheric and Space Sciences and Physics Department, Utah State University, Logan, UT 84322, USA.